



AIAA 2000-1988

**Acoustical and Vortical Interactions
Inside a Channel with Wall Suction**

Todd A. Jankowski and Joseph Majdalani
Marquette University
Milwaukee, WI 53233

6th AIAA/CEAS Aeroacoustics Conference

12–14 June 2000

Lahaina, Hawaii

Acoustical and Vortical Interactions Inside a Channel with Wall Suction

T. A. Jankowski* and J. Majdalani†

Marquette University, Milwaukee, WI 53233

The channel is long and wide. The top and bottom walls are permeable. The head-end is closed and the aft end is wide open. Large suction is imposed uniformly along the permeable walls. The inception of small amplitude harmonic pressure waves gives rise to an oscillatory field that we wish to investigate. The harmonic waves can be either introduced externally or produced internally by random fluctuations in the suction rate. For an isobaric exit, self-triggered acoustic oscillations are of the closed-open type. Based on the normalized pressure-wave amplitude, the conservation equations are linearized and split into leading-order (steady) and first-order (time-dependent) equations. The first-order set is subdivided into an acoustic, pressure-driven, wave equation, and a vortical, boundary-driven, viscous equation. For longitudinal acoustic oscillations, both equations are written at the order of the wall suction Mach number. The resulting equations are then solved in an exact fashion. The novelty lies in the vortical response which can be reduced into a Weber equation following a Liouville-Green transformation. The rotational solution is expressible in terms of confluent hypergeometric functions of the suction flow Reynolds number, Strouhal number, and spatial coordinates. The total solution is thus constructed and found to coincide with the numerical solution of the linearized momentum equation. The oscillatory velocity exhibits similar characteristics to the exact Stokes profile for oscillations in a long channel with hard walls. In particular, a thin rotational layer is observed along with a small velocity overshoot near the wall. Both depth and overshoot are nowhere near their values obtained by switching from suction to injection. In exact contrast to former studies involving injection, the so-called acoustic boundary-layer is found to depreciate when suction is increased or when viscosity is reduced. This response is similar to that of the Stokes layer over hard walls. In all cases, the effect of increasing frequency is consistently found to decrease the rotational layer near the wall.

I. Introduction

THE focus of this paper is to obtain an analytical solution to the oscillatory velocity field in a porous channel with uniform wall suction. The scope is limited to the large suction case for which an exact solution can be obtained for both pressure-driven and boundary-driven temporal velocities. The work is

hoped to increase our understanding of oscillatory and pulsatory flows in porous tubes and channels. Such flows arise in the modeling of the respiratory function in lungs and airways, in the design of hydraulic line transmissions, in sweat cooling, and in flow separation processes. Since oscillatory flows with wall injection have already been analyzed in former studies,¹ the current article will focus on the wall suction case. Another purpose for this study is to serve as a prelude for a generalized formulation that could be applied to oscillatory flow problems with arbitrary levels of suction.

Much work has been invested in the past for the treatment of non-oscillatory flows in rectangular

*Graduate Student and Research Associate. Member AIAA.

†Assistant Professor, Department of Mechanical and Industrial Engineering. Member AIAA.

Copyright © 2000 by T. A. Jankowski and J. Majdalani.
Published by the American Institute of Aeronautics and Astronautics, Inc., with permission.

channels with the same planar geometry considered here. Throughout these studies, numerical, exact or asymptotic mean flow solutions were obtained for different levels of suction or injection along the walls. These formulations were extracted from a single, nonlinear, fourth-order, ordinary differential equation (ODE) that was an exact solution to the Navier-Stokes equations. The fundamental similarity equation was derived by Berman² in his analysis of flows that are bounded by porous surfaces. It depended on the cross-flow Reynolds number ($R = v_w h / \nu$) that was based on the wall suction velocity and the channel's half-height. Berman's landmark paper² set the stage to extensive studies. While some were concerned with developing analytical or numerical mean flow solutions over different ranges of suction (or injection), others have addressed issues regarding solution multiplicity and stability.

With regards to suction flows in rectangular channels, Berman was first in using asymptotic tools to solve the steady flow problem for the small suction case.² Soon after, Yuan,³ Sellars,⁴ and Terrill⁵ developed solutions that extended over increasingly larger ranges of suction. For example, Yuan³ extended Berman's range to $R = 20$, and Sellars⁴ produced one exact solution for $R \rightarrow \infty$. For large suction, Terrill⁵ presented an asymptotic solution that contained viscous corrections of order R^{-1} . As $R \rightarrow \infty$, Terrill's leading-order term reproduced Sellars' exact solution for infinite suction. Note that later studies have indicated that three total solutions could exist for large R .⁶⁻⁸ Two of these solutions, one being stable to temporal perturbations, share the same inviscid leading-order term. In this article, we shall refrain from addressing unstable solutions. In fact, an assumed stable solution will be utilized to represent the mean flowfield.

It should be noted that former mean flow studies have not considered possible fluctuations in the wall suction rate. Such fluctuations can be inevitable and

take place at random frequencies. Those matching the channel's natural frequencies are amplified to the point of promoting a self-sustaining acoustic field. The oscillatory pressure disturbances that are produced give rise to acoustic velocity oscillations that alter the mean flow character. The velocity oscillations stem from both acoustic (pressure-driven) and vorticity (boundary-driven) disturbance modes.⁹ Since no other study seems to have explored the resulting temporal field, it is the purpose of this article to find an analytical solution that can be used to characterize the self-induced oscillatory field in a channel with large wall suction. For cases that involve externally induced oscillations (as opposed to self-triggered oscillations), the same analysis presented here can be employed.

The mathematical modeling starts in Sec. II with a definition of the system geometry. This is followed by a listing of pertinent assumptions, including a description of the mean flow solution that is to be used. In Sec. III, the governing equations are presented and decomposed into mean and time-dependent sets. Section IV deals with the temporal set, which is further broken down into an acoustic and a vortical component. The pressure-driven response is dealt with immediately, while the rotational component is left to be evaluated in Sec. V. There, an exact solution to the vortical momentum equation is derived, following a Liouville-Green transformation that is applied to the normal boundary-layer equation. The attainment of the vortical set completes the solution for the oscillatory velocity which is described in Sec. VI.

II. Defining the Basic Flow Model

A. The Porous Channel

We consider a long slender channel with porous walls that are separated by a distance $2h$. Fluid is withdrawn from the porous surfaces at a uniform wall velocity v_w . Having defined the length and width of the channel as L and w , we make the assumption of a

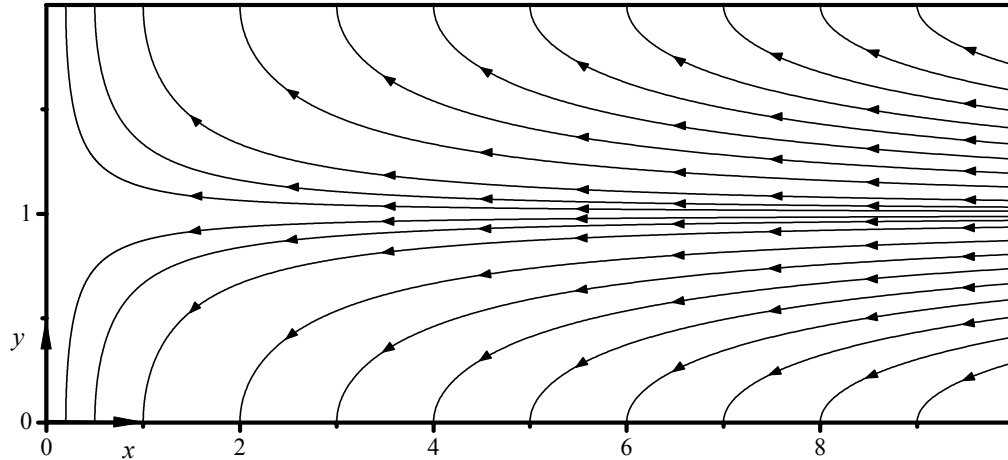


Fig. 1 System geometry showing select mean flow streamlines and velocity vector scales.

two-dimensional planar flow by imposing the condition $w \gg h$. In fact, Terrill⁵ has shown that when the ratio of the width to the height of the channel is $w/h \geq 8$, the presence of lateral walls can be ignored. The system can be further simplified by imposing the condition of symmetry about the channel's midsection plane. This enables us to reduce the solution domain to one half its original size. By way of illustration, a cross section of the channel is shown in Fig. 1. For a symmetric low aspect ratio channel, one can ignore variations in the z -direction and reduce the solution domain to $0 \leq x \leq l$, and $0 \leq y \leq 1$, where $l = L/h$ is the dimensionless channel length.

Under the influence of small variations in the suction rate, a channel that is rigid at the head end and isobarically open at the aft end can develop longitudinal pressure oscillations of amplitude A . The system's acoustic frequency can be specified by

$$\omega_s = (m - 1/2)\pi a_s / L, \quad (1)$$

where a_s refers to the stagnation speed of sound, and m is the oscillation mode number.

B. Limiting Conditions

In order to simplify the analysis to the point where an analytical solution can be attempted, several restrictions must be observed. First, the mean flow is assumed to

be laminar. The mechanisms of mixing, swirling, or turbulence are also discounted. Constant thermostatic properties are used, and the oscillatory pressure amplitude is taken to be small in comparison to the stagnation pressure. Finally, owing to the fact that the mean flow is obtained for an infinitely large Reynolds number, our solutions are limited to $10 < R < \infty$.

C. The Steady Sellars Flow

The mean flow solution can be obtained by employing the similarity parameter suggested by Berman.² In the absence of small amplitude pressure disturbances, the Navier-Stokes can be solved exactly through the use of the steady stream function

$$\Psi = -xF(y). \quad (2)$$

Defining $\mathbf{u}_0 = (u_0, v_0)$ to be the mean velocity vector normalized by v_w , one can express the components of \mathbf{u}_0 as $(u_0, v_0) = (-xF', F)$. The separable component F must satisfy Berman's equation

$$F^{iv} + R(F'F'' - FF''') = 0, \quad (3)$$

with

$$F'(0) = F(1) = F''(1) = 0, \quad F(0) = -1. \quad (4)$$

For a study concerned large suction, we consider the case investigated by Sellars⁴, Terrill⁵, and Zaturka et al.⁶ for which $F = y - 1$. This solution proves to be

exact for $R \rightarrow \infty$. With this choice of F , the velocity and vorticity fields can be written as

$$\mathbf{u}_0 = (-x, y - 1), \quad \nabla \times \mathbf{u}_0 = 0. \quad (5)$$

The foregoing mean flow solution satisfies all the boundary conditions, including the no-slip at the wall. After normalizing the mean pressure by γp_s , (where γ is the ratio of specific heats, and p_s is the stagnation pressure), the complete momentum equation becomes

$$M^2 \mathbf{u}_0 \cdot \nabla \mathbf{u}_0 = -\nabla p_0 + R^{-1} [4\nabla(\nabla \cdot \mathbf{u}_0) - \nabla \times (\nabla \times \mathbf{u}_0)]. \quad (6)$$

Integration gives

$$p_0 = \gamma^{-1} - \frac{1}{2} M^2 [x^2 + (y - 1)^2]. \quad (7)$$

III. Governing Equations

A. Normalized Navier-Stokes

In order to express the differential conservation principles, we evoke dimensionless parameters and see that spatial coordinates are normalized by h , the total instantaneous velocity is normalized by a_s , and time is referenced to the system's oscillation frequency ω_s . Employing asterisks to represent dimensional variables, spatial and temporal coordinates, velocity, pressure and density can be set as

$$x = x^*/h, \quad y = y^*/h, \quad t = \omega_s t^*, \quad \mathbf{u} = \mathbf{u}^*/a_s, \\ p = p^*/\gamma p_s \text{ and } \rho = \rho^*/\rho_s, \quad (8)$$

where ρ_s is the stagnation density. Following this choice, the equations of continuity and motion can be expressed in the non-dimensional form

$$\omega \partial \rho / \partial t + \nabla \cdot (\rho \mathbf{u}) = 0, \quad (9) \\ \rho [\omega \partial \mathbf{u} / \partial t + (\mathbf{u} \cdot \nabla) \mathbf{u}] \\ = -\nabla p + M \varepsilon [4\nabla(\nabla \cdot \mathbf{u}) / 3 - \nabla \times (\nabla \times \mathbf{u})]. \quad (10)$$

Equations (9)–(10) follow the definitions of the non-dimensional frequency $\omega \equiv \omega_s h / a_s$, the suction Mach number $M \equiv v_w / a_s$, and the small parameter $\varepsilon \equiv 1 / R$.

B. Perturbed Variables

With the introduction of small amplitude oscillations at a frequency ω_s , the instantaneous pressure can be expressed as the linear sum of the time-dependent and steady components:

$$p(x, y, t) = 1 / \gamma + \bar{\varepsilon} p_1(x, y) \exp(-it) + \mathcal{O}(M^2 x^2), \quad (11)$$

where $i = \sqrt{-1}$ and $\bar{\varepsilon} = A / (\gamma p_s)$ is the pressure wave amplitude. Expressing the density in the same manner, one gets

$$\rho(x, y, t) = 1 + \bar{\varepsilon} \rho_1(x, y) \exp(-it). \quad (12)$$

Following Lighthill¹⁰ in the assumption of small oscillations, the total velocity can be expanded as

$$\mathbf{u}(x, y, t) = M \mathbf{u}_0(x, y) + \bar{\varepsilon} \mathbf{u}_1(x, y) \exp(-it). \quad (13)$$

C. Total Field Decomposition

Equations (11)–(13) must be inserted back into Eqs. (9)–(10). The zero-order terms yield the mean flow equations. Likewise, $\mathcal{O}(\bar{\varepsilon})$ terms result in

$$-i\omega \rho_1 + \nabla \cdot \mathbf{u}_1 = -M \nabla \cdot (\rho_1 \mathbf{u}_0), \quad (14) \\ -i\omega \mathbf{u}_1 \\ = -M [\nabla(\mathbf{u}_0 \cdot \mathbf{u}_1) - \mathbf{u}_1 \times (\nabla \times \mathbf{u}_0) - \mathbf{u}_0 \times (\nabla \times \mathbf{u}_1)] \\ -\nabla p_1 + M \varepsilon [4\nabla(\nabla \cdot \mathbf{u}_1) / 3 - \nabla \times (\nabla \times \mathbf{u}_1)]. \quad (15)$$

Equations (14) and (15) describe the intimate coupling between mean and steady motions. They clearly indicate that the mean velocity \mathbf{u}_0 has a strong influence on the oscillatory flow component.

IV. Temporal Field Decomposition

A. Irrotational and Solenoidal Vectors

In order to proceed, the temporal disturbances are split into solenoidal and irrotational components. Using a circumflex to denote the curl-free pressure-driven part, and a tilde for the divergence-free boundary-driven part, the time-dependent velocity component can be expressed as

$$\mathbf{u}_1 = \hat{\mathbf{u}} + \tilde{\mathbf{u}} \quad (16)$$

with $\Omega_1 = \nabla \times \mathbf{u}_1 = \nabla \times \tilde{\mathbf{u}}$, $p_1 = \hat{p}$, $\rho_1 = \hat{\rho}$. (17)

The decomposition charges all vortices to the solenoidal field, and compressibility sources and sinks to the irrotational field. Such decomposition is based on a fundamental theorem of vector analysis that was first addressed by Stokes¹¹ in 1849 and proven rigorously by Blumenthal in 1905. Furthermore, the theorem is at the root of Helmholtz's work on vortex motion in 1858 and is of great importance in both fluid dynamic and electromagnetic theories.

B. The Linearized Navier-Stokes Equations

Insertion of Eqs. (16)-(17) into Eqs. (14)-(15) leads to two independent sets that are only coupled through existing boundary conditions. One set that we call acoustic is compressible and irrotational; the other, we call vortical, is incompressible and rotational. These responses are byproducts of pressure-driven and vorticity-driven oscillation modes at $\mathcal{O}(\bar{\varepsilon})$.

1. *The Acoustic Set*

$$-i\omega\hat{p} + \nabla \cdot \hat{\mathbf{u}} = -M\nabla \cdot (\hat{\rho}\mathbf{u}_0), \tag{18}$$

$$-i\omega\hat{\mathbf{u}} = -\nabla\hat{p} + 4M\varepsilon\nabla^2(\nabla \cdot \hat{\mathbf{u}})/3 - M[\nabla(\hat{\mathbf{u}} \cdot \mathbf{u}_0) - \hat{\mathbf{u}} \times (\nabla \times \mathbf{u}_0)]. \tag{19}$$

2. *The Vortical Set*

$$\nabla \cdot \tilde{\mathbf{u}} = 0, \tag{20}$$

$$-i\omega\tilde{\mathbf{u}} = -M\varepsilon\nabla \times (\nabla \times \tilde{\mathbf{u}}) - M[\nabla(\tilde{\mathbf{u}} \cdot \mathbf{u}_0) - \tilde{\mathbf{u}} \times (\nabla \times \mathbf{u}_0) - \mathbf{u}_0 \times (\nabla \times \tilde{\mathbf{u}})]. \tag{21}$$

C. Coupling Conditions

Two boundary conditions must be satisfied by the unsteady velocity component \mathbf{u}_1 . These are the no-slip condition at the wall $u_1(x, 0) = 0$, and symmetry about the midsection plane, $\partial u_1(x, 1)/\partial y = 0$.

D. Acoustic Solution

As we multiply Eq. (18) by $-i\omega$, take the divergence of Eq. (19), and add resulting terms, a wave equation is produced:

$$\nabla^2\hat{p} + \omega^2\hat{p} = -4M\varepsilon\nabla^2(\nabla \cdot \hat{\mathbf{u}})/3 - M\{i\omega\nabla \cdot (\mathbf{u}_0\hat{p}) - \nabla^2(\hat{\mathbf{u}} \cdot \mathbf{u}_0) + \nabla \cdot [\hat{\mathbf{u}} \times (\nabla \times \mathbf{u}_0)]\}. \tag{22}$$

A solution, at $\mathcal{O}(M)$, can be achieved through the use of separation of variables. This solution, corresponding to longitudinal oscillations, is obtainable through the use of the rigid wall boundary conditions. At the oustet, the acoustic pressure and velocity are

$$\hat{p} = \cos(\omega x) + \mathcal{O}(M), \tag{23}$$

$$\hat{\mathbf{u}} = i \sin(\omega x)\hat{\mathbf{i}} + \mathcal{O}(M). \tag{24}$$

E. Vortical Equations

Assuming that the ratio of the normal to axial velocity is of the same order as the Mach number (i.e. $\tilde{v}/\tilde{u} = \mathcal{O}(M)$), \tilde{v} can be neglected. This assumption can be justified in view of the arguments presented by Flandro¹² and Majdalani and Van Moorhem.¹ Applying this condition, along with the definition of the mean flow velocity, the axial momentum equation can be expressed as

$$iSr\tilde{u} = \frac{\partial}{\partial x}(\tilde{u}u_0) + v_0\frac{\partial\tilde{u}}{\partial y} - \varepsilon\frac{\partial^2\tilde{u}}{\partial y^2} + \mathcal{O}(M), \tag{25}$$

where $Sr \equiv \omega/M$ is the Strouhal number. For large suction, Eq. (25) becomes

$$iSr\tilde{u} = (y-1)\frac{\partial\tilde{u}}{\partial y} - x\frac{\partial\tilde{u}}{\partial x} - \tilde{u} - \varepsilon\frac{\partial^2\tilde{u}}{\partial y^2} + \mathcal{O}(M). \tag{26}$$

An exact solution to Eq. (26) is presented next.

V. The Exact Solution

A. The Separable Boundary-Layer Equation

An exact solution to Eq. (26) can be achieved through the use of separation of variables. Assuming the form

$$\tilde{u}(x, y) = X(x)Y(y), \quad (27)$$

substitution into Eq. (26) leads to

$$\frac{x}{X} \frac{dX}{dx} = \frac{(y-1)}{Y} \frac{dY}{dy} - \frac{\varepsilon}{Y} \frac{d^2Y}{dy^2} - iSr - 1 = \kappa_n \quad (28)$$

where $\kappa_n > 0$ is the separation eigenvalue. Integration of the x -equation can be performed easily and then inserted into Eq. (27). The solution becomes

$$\tilde{u}(x, y) = \sum_n c_n x^{\kappa_n} Y_n(y), \quad (29)$$

where c_n is an integration constant associated with κ_n . Satisfaction of the no-slip boundary condition at the wall requires setting the acoustic and vortical velocity components equal and opposite at $y = 0$. One finds

$$\tilde{u}(x, 0) = -i \sin(\omega x). \quad (30)$$

Using a series expansion of the sine function, and setting the result equal to Eq. (29), one gets

$$\sum_n c_n x^{\kappa_n} Y_n(0) = -i \sum_{n=0}^{\infty} \frac{(-1)^n (\omega x)^{2n+1}}{(2n+1)!}. \quad (31)$$

Equating terms yields

$$\kappa_n = 2n + 1, \quad c_n = -i \frac{(-1)^n \omega^{2n+1}}{(2n+1)!}, \quad Y_n(0) = 1, \quad (32)$$

where $n = 0, 1, 2, \dots, \infty$. The expression for the rotational component becomes

$$\tilde{u}(x, y) = -i \sum_{n=0}^{\infty} \frac{(-1)^n (\omega x)^{2n+1}}{(2n+1)!} Y_n. \quad (33)$$

In order to complete Eq. (33), Y_n needs to be determined from Eq. (28). The search for Y_n leads to a boundary-value problem of the form

$$\varepsilon \frac{d^2 Y_n}{dy^2} - (y-1) \frac{dY_n}{dy} + [iSr + 2n + 2] Y_n = 0 \quad (34)$$

that is subject to

$$Y_n(0) = 0, \quad Y_n'(1) = 0. \quad (35)$$

The two boundary conditions stem from the no slip and core symmetry requirements.

B. The Liouville-Green Transformation

Careful examination of Eq. (34) leads us to believe that an exact solution is tractable if the equation is first transformed from a variable coefficient ODE, to an

equation with constant coefficients. Working toward that end, the Liouville-Green transformation is applied by first setting $r = 1 - y$. This transforms Eq.(34) into

$$\varepsilon \frac{d^2 Y_n}{dr^2} - r \frac{dY_n}{dr} + [iSr + 2n + 2] Y_n = 0, \quad (36)$$

with boundary conditions $Y_n(1) = 0$ and $Y_n'(0) = 0$. Next, we define

$$X = \phi(r), \quad B(X) = \psi(r) Y_n(r). \quad (37)$$

These change the derivatives of Y_n into

$$\frac{dY_n}{dr} = -\frac{\psi'}{\psi^2} B + \frac{1}{\psi} \frac{dB}{dX} \frac{dX}{dr} = -\frac{\psi'}{\psi^2} B + \frac{\phi'}{\psi} \frac{dB}{dX} \quad (38)$$

$$\begin{aligned} \frac{d^2 Y_n}{dr^2} &= \frac{\phi'^2}{\psi} \frac{d^2 B}{dX^2} + \left(\frac{\phi''}{\psi} - \frac{2\phi'\psi'}{\psi^2} \right) \frac{dB}{dX} \\ &\quad - \left(\frac{\psi''}{\psi^2} - \frac{2\psi'^2}{\psi^3} \right) B, \end{aligned} \quad (39)$$

where primes stand for differentiation with respect to r . Substitution of these derivatives into Eq. (36) gives

$$\begin{aligned} \frac{d^2 B}{dX^2} + \frac{1}{\phi'^2} \left(\phi'' - \frac{2\phi'\psi'}{\psi} - rR\phi' \right) \frac{dB}{dX} \\ + \frac{1}{\phi'^2} \left(-\frac{\psi''}{\psi} + \frac{2\psi'^2}{\psi^2} + \frac{rR\psi'}{\psi} \right) B \\ + \frac{1}{\phi'^2} (R[iSr + (2n + 2)]) B = 0. \end{aligned} \quad (40)$$

The functions ψ and ϕ are now chosen to force the variable coefficients in the transformed equation to be constant values. To do this, the coefficient of the first derivative term is set equal to zero

$$\phi'' - \frac{2\phi'\psi'}{\psi} - rR\phi' = 0, \quad \frac{\psi'}{\psi} = \left(\frac{\phi''}{\phi'} - rR \right) / 2. \quad (41)$$

Integrating gives $\psi = H_0 \sqrt{\phi'} \exp(-Rr^2/4)$, where H_0 is a constant. Equation (40) simplifies into

$$\frac{d^2 B}{dX^2} + \left\{ \frac{R}{\phi'^2} [iSr - (2n + 2)] + \delta \right\} B = 0; \quad (42)$$

$$\text{where} \quad \delta = \frac{1}{\phi'^2} \left(-\frac{\psi''}{\psi} + \frac{2\psi'^2}{\psi^2} + \frac{rR\psi'}{\psi} \right) \quad (43)$$

By imposing

$$\frac{R}{\phi'^2} [iSr + (2n + 2)] = \text{constant}, \quad (44)$$

one obtains

$$\phi' = \sqrt{R} \text{ and } X = \phi = r\sqrt{R}. \quad (45)$$

Furthermore, setting $H_0 = 1/\sqrt[4]{R}$ gives

$$\psi(r) = \exp(-Rr^2/4). \quad (46)$$

Finally, the transformed equation, and corresponding boundary conditions become

$$\frac{d^2 B}{dX^2} + (p + \frac{1}{2} - \frac{1}{4}X^2)B = 0; \quad p = 2 + 2n + iSr \quad (47)$$

$$\text{with } B(\sqrt{R}) = \exp(-R/4); \quad \frac{dB(0)}{dX} = 0. \quad (48)$$

C. The Complete Solution

Equation (47) is a Weber differential equation. This type is known to have independent solutions that are parabolic cylinder functions of the form

$$B(X) = K_1 D_p(X) + K_2 D_p(-X). \quad (49)$$

Due to the complexity of the parabolic cylinder functions, symbolic programming is employed to evaluate the constants K_1 and K_2 . This is done in fulfillment of the boundary conditions given by Eq. (48). The result is

$$K_1 = K_2 = 2^{-1-p/2} \Gamma\left(\frac{1-p}{2}\right) / [\sqrt{\pi} \Phi(-\frac{1}{2}p, \frac{1}{2}, \frac{1}{2}R)], \quad (50)$$

where Γ is Euler's Gamma function and Φ is the confluent hypergeometric function. The latter is expandable in a series of the type

$$\Phi(a, b; x) = 1 + \frac{a}{b} \frac{x}{1!} + \frac{a(a+1)}{b(b+1)} \frac{x^2}{2!} + \frac{a(a+1)(a+2)}{b(b+1)(b+2)} \frac{x^3}{3!} + \dots \quad (51)$$

Substitution of Eqs. (49) and (50) into Eq. (37) leads to

$$Y_n(r) = \frac{\Phi(-\frac{1}{2}p, \frac{1}{2}, \frac{1}{2}Rr^2)}{\Phi(-\frac{1}{2}p, \frac{1}{2}, \frac{1}{2}R)}. \quad (52)$$

One may now revert back to original variables and revisit Eq. (33). One finds

$$\tilde{u} = -i \sum_{n=0}^{\infty} \frac{(-1)^n (\omega x)^{2n+1} \Phi[-\frac{1}{2}p, \frac{1}{2}, \frac{1}{2}R(y-1)^2]}{(2n+1)! \Phi(-\frac{1}{2}p, \frac{1}{2}, \frac{1}{2}R)}. \quad (53)$$

Using continuity, the normal component of the rotational velocity can now be deduced. From Eq. (20) we have

$$\begin{aligned} \tilde{v} &= - \int \frac{\partial \tilde{u}}{\partial x} dy \\ &= -i\omega r \sum_{n=0}^{\infty} \frac{(-1)^n (\omega x)^{2n} \Phi(-\frac{1}{2}p, \frac{3}{2}, \frac{1}{2}Rr^2)}{(2n)! \Phi(-\frac{1}{2}p, \frac{1}{2}, \frac{1}{2}R)}. \end{aligned} \quad (54)$$

In view of Eqs. (53)–(54), the total oscillatory velocity can now be constructed by summing both acoustical and vortical components. At length, one obtains

$$u_1 = i \left[\sin(\omega x) - \sum_{n=0}^{\infty} \frac{(-1)^n (\omega x)^{2n+1} \Phi(a, b, \frac{1}{2}RF^2)}{(2n+1)! \Phi(a, b, \frac{1}{2}R)} \right], \quad (55)$$

$$v_1 = i\omega F \sum_{n=0}^{\infty} \frac{(-1)^n (\omega x)^{2n} \Phi(a, c, \frac{1}{2}RF^2)}{(2n)! \Phi(a, b, \frac{1}{2}R)}, \quad (56)$$

with $a = -1 - n - \frac{1}{2}iSr$, $b = \frac{1}{2}$, and $c = \frac{3}{2}$.

D. Numerical verification

The analytical solution that we constructed can be easily verified via comparisons with the numerical solution of Eq. (26). This can be accomplished using the same numerical code that was developed by Majdalani and Van Moorhem¹ for the injection case. For large suction, we obtain a uniform agreement of at least six significant digits using a step size of $\Delta y = 5 \times 10^{-6}$. Note that, for injection, numerical predictions acquired from the same code were shown, in previous studies,^{1,13} to agree with both asymptotic and experimental observations.

Comparing the numerical output to the exact solution of the linearized momentum equation (Eq. (26)) serves a dual purpose. First, it increases our confidence in the numerical algorithm that was currently used to integrate the momentum equation. Second it ensures the correctness of the procedure that led to the exact solution.

VI. Discussion

Based on Eq. (55), the time evolution of the axial oscillatory velocity component is analyzed in Figs. 2–4

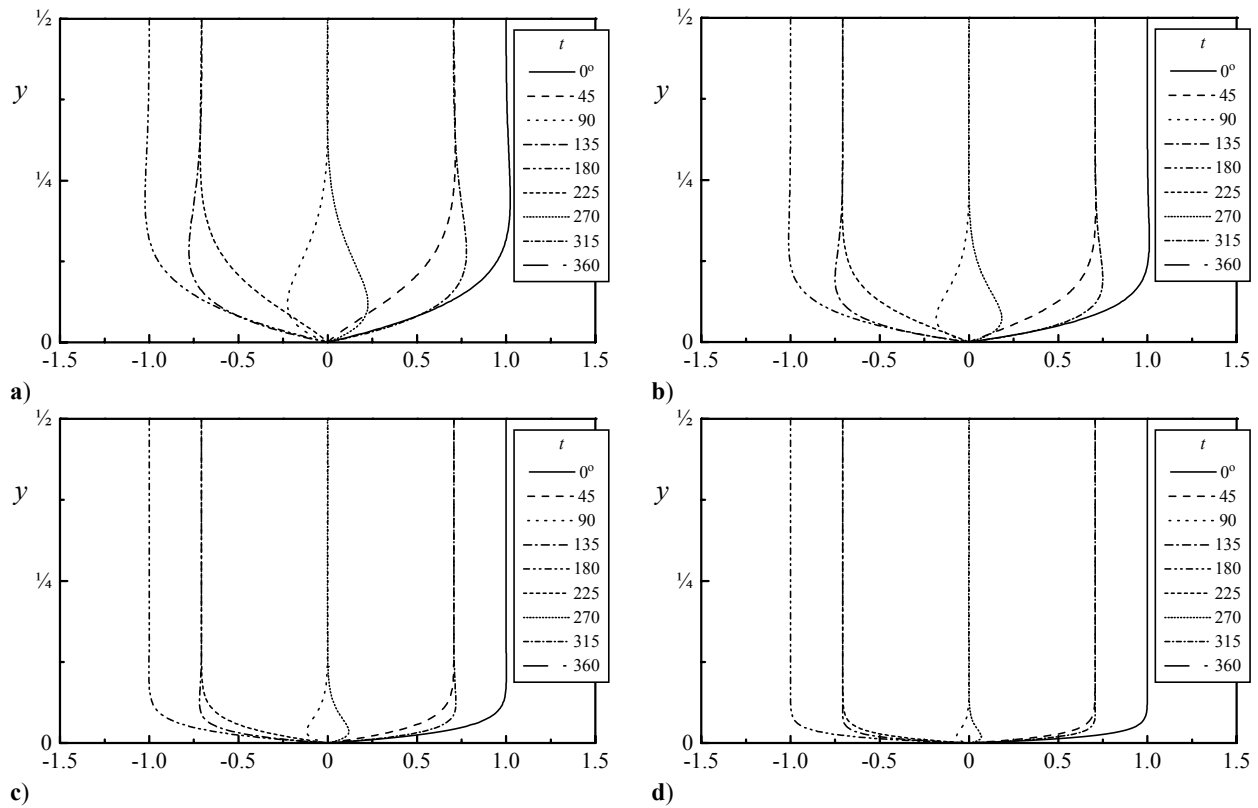


Fig. 2 The oscillatory velocity $u_1 \exp(-it)$ plotted at eight different times for $m = 1$, $x/l = 1$, $Sr = 20$, and a) $R = 10$, b) $R = 20$, c) $R = 50$, and d) $R = 100$. This can be due to a progressive decrease in viscosity.

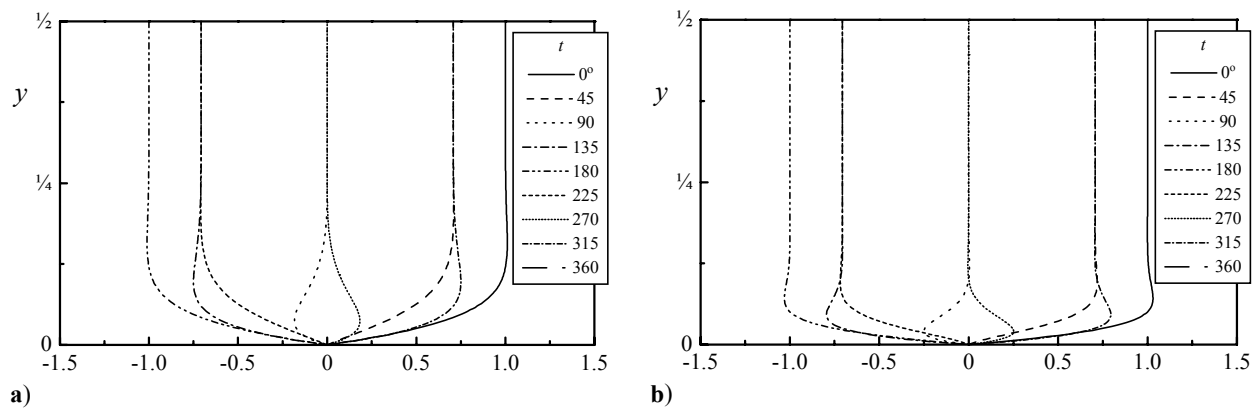


Fig. 3 The oscillatory velocity $u_1 \exp(-it)$ plotted at eight different times for $x/l = 1$, $R = 20$, and $m = 1$. Properties correspond to a) $Sr = 10$, and b) $Sr = 100$. This variation is due to an order of magnitude increase in oscillation frequency. Higher Sr increase the overshoot while reducing the penetration depth.

over a range of parameters. At first glance, the profiles seem to concur with classical theory of time-dependent flows that is fairly well-presented in a survey by Rott.¹⁴ In fact, a strong resemblance is found between our solution and the oscillatory flow solution over non-

permeable walls. As such, the velocity appears to be a traveling wave with two distinct components. A viscous, rotational component that is dominant near the wall, and an inviscid, acoustic part that is retained near the core. While their sum satisfies the no slip at the

wall, the rotational part decays as the distance from the wall is increased. The rotational layer and corresponding thickness appear to be largest when viscosity is large and suction is small. The profile also exhibits a small velocity overshoot near the wall. This phenomenon is known as Richardson’s annular effect and is a characteristic of oscillatory flows. It can take place near the wall when rotational and acoustic waves have favorable phases and, hence, additive amplitudes.

In order to illustrate the effect of R on the solution, the suction Reynolds number is increased in Fig. 2 by one order of magnitude while keeping other variables constant. As the Reynolds number is increased, viscous effects become less pronounced: The penetration depth (i.e., rotational boundary-layer) becomes smaller. The Richardson overshoot also diminishes. This effect is to be expected as the convective withdrawal at the wall becomes more appreciable with successive increases in R . Suction seems to inhibit the boundary-layer growth near the wall. This effect is the exact opposite of what has been reported in the presence of injection. As shown by Majdalani^{15,16} increasing injection increases the penetration depth. It also leads to a substantially larger velocity overshoot that averages 50%.

In Fig. 3, the effect of varying the oscillation frequency is captured. Thus, as the Strouhal number is increased from 10 to 100, a slight increase in the

Richardson effect is noted. This is accompanied by a reduction in penetration depth. This observation is consistent with the effect of frequency in the presence of injection. In both cases, it can be shown that increasing frequency increases the temporal velocity near the wall and decreases the penetration depth. The increased overshoot can be attributed to the fact that the normal rotational wavelength is inversely proportional to Sr . A shorter wavelength leads to a vortico-acoustic coupling that is closer to the wall. Since the vortical amplitude increases as we draw nearer to the wall, a larger vortical contribution can be added to the acoustic component at shorter wavelengths.

In Fig. 4, all parameters are fixed except for the suction speed. Hence, as v_w is increased by one order of magnitude, a reduction in penetration depth and breadth (overshoot) are noted. The influence of suction speed on altering the flow character is certainly the greatest. Surveying these figures as a whole suggests that, over a wide range of Reynolds and Strouhal numbers, the boundary-layer at the wall shares several similarities with the classic Stokes layer over hard walls. As opposed to the penetration depth with injection, the rotational boundary-layer here is very thin. The velocity overshoot is also minimal. These characteristics are markedly different from the basic features of an oscillatory flow with wall injection.^{15,16}

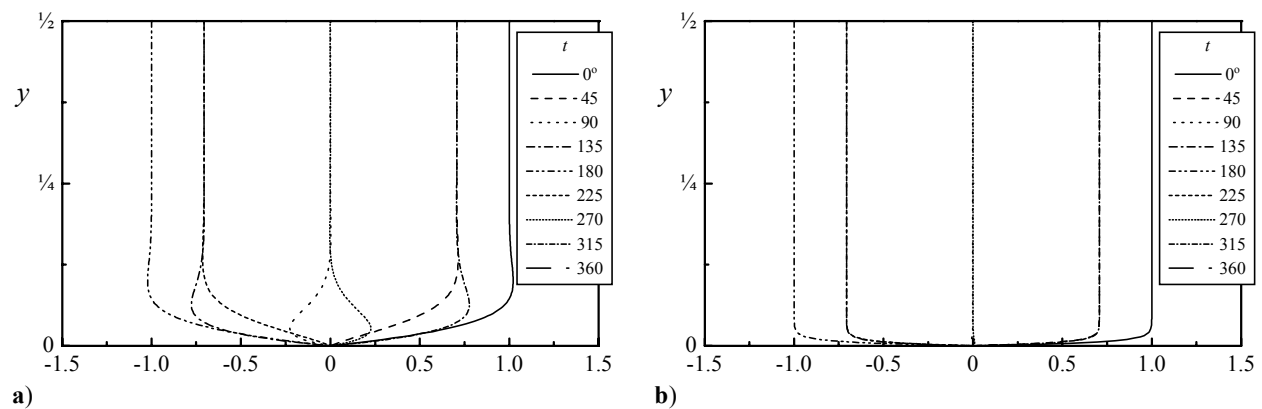


Fig. 4 The oscillatory velocity $u_1 \exp(-it)$ plotted at eight different times for $x/l = 1$, and $m = 1$. Properties correspond to a) $R = 20$, $Sr = 50$, and b) $R = 200$, $Sr = 5$. This variation is due to an order of magnitude increase in suction speed. Clearly, large suction reduces the penetration depth and overshoot.

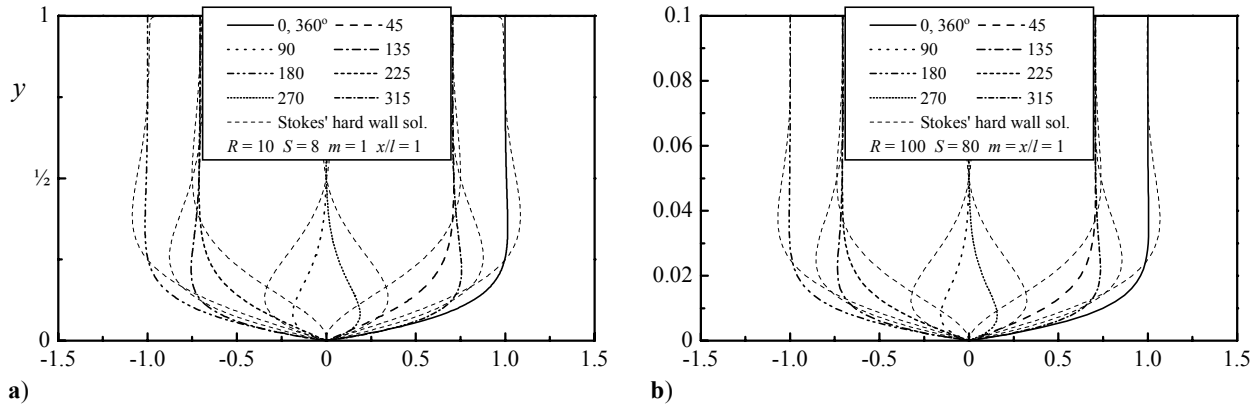


Fig. 5 Comparison between the oscillatory velocities with and without suction. Both $u_1 \exp(-it)$ and the exact Stokes solution (over hard walls) are shown at eight different times for $x/l = 1$, $v_w = 2^{1/6} \sqrt{\omega_s \nu}$, and $m = 1$. Parameters are: a) $R = 10$, $Sr = 8$, and b) $R = 100$, $Sr = 80$. The suction speed is set below Stokes' diffusion speed. Timelines show that the penetration depth and overshoot are reduced with suction.

In order to compare our solution directly to Stokes' exact solution, the suction speed is reduced to a value below the Stokes diffusion speed, $\sqrt{2\omega_s \nu}$. Letting

$$v_w = 2^{1/6} \sqrt{\omega_s \nu}, \quad (57)$$

the Stokes number becomes

$$h \sqrt{\omega_s / 2\nu} = Sr^2 / R. \quad (58)$$

For this condition, the exact Stokes solution can be compared to ours in Fig. 5. As shown for two Reynolds numbers, the presence of suction attracts the shear layers closer to the wall. As a result, both rotational depth and overshoot are reduced when suction is present. The boundary-layer thickness with suction is thus thinner than the traditional Stokes layer.

References

- ¹Majdalani, J., and Van Moorhem, W. K., "Improved Time-Dependent Flowfield Solution for Solid Rocket Motors," *AIAA Journal*, Vol. 36, No. 2, 1998, pp. 241-248.
- ²Berman, A. S., "Laminar Flow in Channels with Porous Walls," *Journal of Applied Physics*, Vol. 24, No. 9, 1953, pp. 1232-1235.
- ³Yuan, S. W., "Further Investigation of Laminar Flow in Channels with Porous Walls," *Journal of Applied Physics*, Vol. 27, No. 3, 1956, pp. 267-269.
- ⁴Sellars, J. R., "Laminar Flow in Channels with Porous Walls at High Suction Reynolds Numbers," *Journal of Applied Physics*, Vol. 26, No. 4, 1955, pp. 489-490.
- ⁵Terrill, R. M., "Laminar Flow in a Uniformly Porous Channel," *The Aeronautical Quarterly*, Vol. 15, 1964, pp. 299-310.
- ⁶Zaturka, M. B., Drazin, P. G., and Banks, W. H. H., "On the Flow of a Viscous Fluid Driven Along a Channel by Suction at Porous Walls," *Fluid Dynamics Research*, Vol. 4, No. 3, 1988, pp. 151-178.
- ⁷Zaturka, M. B., and Banks, W. H. H., "Suction-Driven Flow in a Porous Pipe," *Journal of Applied Mathematics and Mechanics (ZAMM)*, Vol. 75, No. 1, 1995, pp. 21-30.
- ⁸Lu, C., "On the Asymptotic Solution of Laminar Channel Flow with Large Suction," *SIAM Journal on Mathematical Analysis*, Vol. 28, No. 5, 1997, pp. 1113-1134.
- ⁹Chu, B.-T., and Kováczny, L. S. G., "Non-Linear Interactions in a Viscous Heat-Conducting Compressible Gas," *Journal of Fluid Mechanics*, Vol. 3, No. 5, 1957, pp. 494-514.
- ¹⁰Lighthill, M. J., "The Response of Laminar Skin Friction and Heat Transfer to Fluctuations in the Stream Velocity," *Proceedings of the Royal Society, London, Series A*, Vol. 224, 1954, pp. 1-23.
- ¹¹Stokes, G. G., "On the Dynamical Theory of Diffraction," *Mathematical and Physical Papers*, Vol. 2, No. 4, 1883, pp. 243-328.
- ¹²Flandro, G. A., "Effects of Vorticity on Rocket Combustion Stability," *Journal of Propulsion and Power*, Vol. 11, No. 4, 1995, pp. 607-625.
- ¹³Majdalani, J., and Van Moorhem, W. K., "A Multiple-Scales Solution to the Acoustic Boundary Layer in Solid Rocket Motors," *Journal of Propulsion and Power*, Vol. 13, No. 2, 1997, pp. 186-193.

¹⁴Rott, N., "Theory of Time-Dependent Laminar Flows," *High Speed Aerodynamics and Jet Propulsion –Theory of Laminar Flows*, Section D, Vol. IV, edited by F. K. Moore, Princeton University Press, Princeton, New Jersey, 1964, pp. 395-438.

¹⁵Majdalani, J., "The Boundary Layer Structure in Cylindrical Rocket Motors," *AIAA Journal*, Vol. 37, No. 4, 1999, pp. 505-508.

¹⁶Majdalani, J., "Asymptotic Formulation for an Acoustically Driven Field Inside a Rectangular Cavity with a Well-defined Convective Mean Flow Motion," *Journal of Sound and Vibration*, Vol. 223, No. 1, 1999, pp. 73-95.